

Received 21 May 2024; accepted 6 June 2024. Date of publication 13 June 2024; date of current version 24 September 2024.

Digital Object Identifier 10.1109/OJCOMS.2024.3414193

Peak Age of Information Optimization in Heterogeneous Aloha Networks

DEWEI WU^{ID}¹, WEN ZHAN^{ID}¹ (Member, IEEE), XINGHUA SUN^{ID}¹ (Member, IEEE),
JINGJING LIU^{ID}¹ (Member, IEEE), AND ZHIHENG LI²

¹School of Electronics and Communication Engineering, Sun Yat-sen University (Shenzhen), Shenzhen 518107, Guangdong, China

²School of Mathematical Sciences, University of Science and Technology of China, Hefei 230026, Anhui, China

CORRESPONDING AUTHOR: W. ZHAN (e-mail: zhanw6@mail.sysu.edu.cn)

The work of Wen Zhan was supported in part by the Shenzhen Science and Technology Program under Grant RCBS20210706092408010; in part by the Open Fund of State Key Laboratory of Satellite Navigation System and Equipment Technology under Grant CEPNT-2021KF-04; and in part by the Science and Technology Planning Project of Key Laboratory of Advanced IntelliSense Technology, Guangdong Science and Technology Department under Grant 2023B1212060024. The work of Xinghua Sun was supported by the Guangdong Basic and Applied Basic Research Foundation under Grant 2024A1515012015. The work of Jingjing Liu was supported by the National Natural Science Foundation of China under Grant 62174181.

ABSTRACT Rapid advancements in Internet of Things (IoT) technology have promoted numerous novel applications that are sensitive to information timeliness. With different applications coexisting in one wireless network, each of which has heterogeneous traffic characteristics, it is of paramount importance while challenging to address how to characterize and optimize the information freshness performance network-wide, particularly in the massive access scenario. This paper casts attention on the heterogeneous slotted Aloha network and uses the Peak Age of Information (PAoI) metric to quantify information freshness. By assuming that the sensors in each group are equipped with unit-sized buffers and Bernoulli packet arrival, we derive the network steady-state point and PAoI. Depending on whether one group or all groups are age-sensitive, we focus on single-group PAoI and global PAoI optimization respectively. When only one single group is age-sensitive, we derive its optimal transmission probability. When all groups are age-sensitive, we propose a heuristic algorithm based on the particle swarm optimization method, where the bi-stability of Aloha network is considered for avoiding the risk of rapid performance deterioration. Extensive simulation results are presented to verify our analysis and the effectiveness of the proposed algorithm.

INDEX TERMS Aloha, age of information, heterogeneous networks, random access.

I. INTRODUCTION

APID advancing Internet of Things (IoT) has driven the growth of numerous applications that are time-sensitive to the received information. Such applications include healthcare [1], industrial control [2], environmental monitoring [3], and vehicular networks [4]. For instance, timely medical information is crucial to guarantee the safety of remote surgery [5], timely detection and alerting of irregular states in industrial control and environmental monitoring can avoid unnecessary losses [6], [7], and the timeliness of status information interaction in vehicular

networks is critical to the reliability of all vehicles [8]. In these scenarios, the freshness of the received information will directly affect the performance of the application due to the strict demand on information timeliness [9].

Driven by many emerging IoT applications [10], Age of Information (AoI) was first proposed in [11] to characterize the information timeliness, which measures the time elapsed since the generation of the most recent successfully received update at the destination. The Peak Age of Information (PAoI), which is defined as the maximum AoI attained before receiving a packet [12], is of interest in applications with

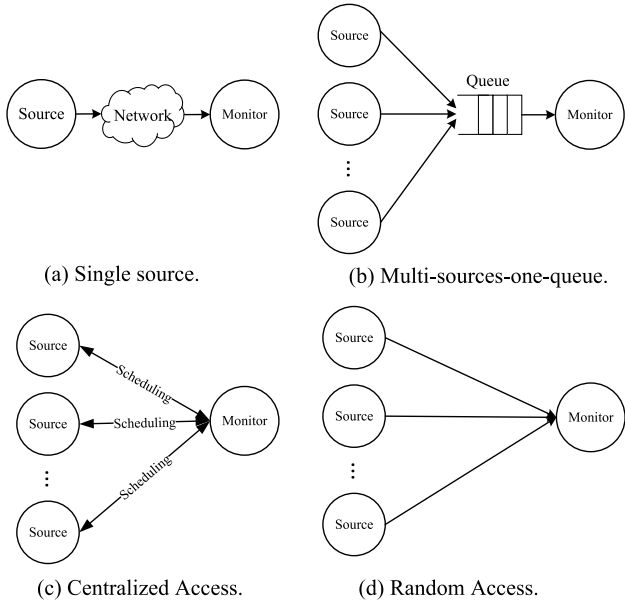


FIGURE 1. Different types of communication scenarios in related works: (a) Single source scenario. (b) Multiple sources with service queue scenario. (c) Multiple sources scenario with centralized access. (d) Multiple sources scenario with random access.

timeliness threshold limitations in IoT [13], [14], [15], [16] and will be the main focus of this paper.

A. RELATED WORK

By definition, the AoI distinguishes itself from the traditional metrics, such as delay and throughput, in that there are functions of how many packets are transmitted and how much delay packets experience since each packet is generated. This novel metric can ensure the information timeliness for different communication systems and has received spiraling attention in recent years.

Related works can be traced back to the single source-monitor scenario, as shown in Fig. 1a, in which one source periodically sends updates via a wired or wireless network to a remote monitor. The single source monitor scenario has been extensively studied, where the focus was on deriving the average AoI and PAoI based on a wide range of classical queueing models with different distributions of packet arrival and service time [11], [12], [17], [18], [19], [20], [21]. Specifically, the authors of [11] analyzed the average AoI of the M/M/1 queue with FCFS discipline, and the work [12] analyzed the PAoI of this queue and extended to the case with LCFS discipline. The study [17] investigated the average AoI of the queues M/M/2, M/M/ ∞ . The AoI performance of other continuous-time queues such as M/D/1 and D/M/1 are analyzed and summarized in [18], while of discrete-time queues such as Geo/Geo/1, are derived in [19]. The AoI and PAoI of multiple point-to-point queues coexisting in the same space are analyzed in [20], [21].

Apart from the single-source scenarios, the multi-sources-one-queue model as illustrated in Fig. 1(b) has also attracted great interest, where multiple sources transmit their packets

to a common server and packets are queued on the server side. Many studies focus on how to characterize the average AoI and PAoI in multiple sources scenario [22], [23], [24], [25]. Specifically, the work [22] considered a status update system where multiple sources coexist with different packet generation rates, and numerically obtained the distributions of AoI and PAoI in a matrix-geometric form. The work [23] found the region of feasible AoI for multiple-sources-one-queue model, and derived a method for calculating the AoI in finite-state queueing systems based on stochastic hybrid systems. The AoI and PAoI in a multi-class M/G/1 queueing system were derived and optimized by the bisection algorithm in [24]. The AoI in multi-class M/G/1 queue was investigated in [25], and the author considered the homogeneous and heterogeneous sources separately. For the homogeneous cases, the average AoI with age weight factors of different streams was considered and the input rate allocation strategy, given the total input rate and service rate, was presented. For the heterogeneous case, the sum of AoI in a two-stream system with a fixed total input rate is optimized by the input rate allocation.

A more general communication scenario, as Fig. 1(c) illustrated, is the multiple sources with centralized access, where packets are generated or transmitted by the decision from the base station. Specifically, the work [26] investigated the long-term average AoI minimization in an energy harvesting system. The AoI minimization by scheduling algorithms in the loss network was analyzed in [27], where arriving packets that cannot be served upon arrival get lost. A scheduling algorithm named Juventas was proposed in [28] for minimizing the AoI in a heterogeneous network with different sample sizes. The study [29] proposed an online algorithm for minimizing the AoI in a multi-access edge computing-assisted status update system with heterogeneous energy harvesting devices. The work [30] regarded the multi-sources-one-queue as one gateway and improved the PAoI in a heterogeneous satellite network with multiple gateways by a D3QN-based age-oriented access control strategy. Note that [26], [27], [28], [29], [30] optimizes the age performance through centralized scheduling, which leads to significant signaling overhead in wireless communication and is not aligned with the low-cost and energy-efficient requirements of many practical IoT services. For large-scale IoT with a large number of deployed sensors, distributed random access protocols, where individual sensors make independent decisions on whether to transmit or not, have proven to be a simpler yet more elegant solution.

Random access network is illustrated in Fig. 1d, where multiple sources make the transmission decision independently. As a popular distributed random access scheme with minimum coordination, Aloha has gained popularity in IoT-oriented wireless networks like LoRa [31] and NB-IoT [32]. The age performance of Aloha networks has been investigated in [33], [34], [35], [36], [37], [38], where they focused on the homogeneous sources and revealed that the age performance of network is closely related to the

network size and the channel access probability of sources. However, the homogeneous network is inconsistent with the existence of different quality of service requirements for the various coexisting applications in IoT. For example, the AoI-sensitive sensors coexist in the same network with the AoI-insensitive application nodes [39], [40]. In addition to the homogeneous Aloha networks, the heterogeneous Aloha networks, where the number of sources and parameter settings (e.g., the access probability and the input rate) from each group are different, are more worthy of our attention.

To characterize and further optimize the AoI and PAoI performance in heterogeneous Aloha networks, the authors in [41] considered how to guarantee the stability of the queue of one application node when optimizing AoI for another sensor node. The work [42] analyzed the effect of transmission probability tuning of one sensor on its own AoI concerning another node's delay by numerical simulation results. The work [43] focused on the AoI minimization of one user in the cognitive radio network, where two secondary node shares the primary node spectrum through the underlay scheme. Although the above heterogeneous Aloha network work characterizes or optimizes AoI for one node with information timeliness requirements, the network size is limited to at most three nodes. How to characterize and further optimize age performance for heterogeneous Aloha networks with larger network scales is still an open question. In addition, the above studies [41], [42], [43] for heterogeneous Aloha networks only have one single information source pursuing optimal AoI. In this regard, multiple heterogeneous application groups in IoT may all have a demand for information timeliness [44], and it is worthwhile to optimize the age performance for all coexisting application groups in heterogeneous Aloha networks.

B. CONTRIBUTIONS

To solve the above problems, we consider an Aloha network with multiple heterogeneous groups of applications, each of them has its own packet arrival rate and the number of sensors. The sensor of each group is equipped with a unit-size buffer and the packet arrival process follows the Bernoulli distribution. Our contributions are summarized as follows:

- *PAoI Analysis:* By analyzing the behavior of head-of-line packets, we obtain the fixed-point equation for the heterogeneous Aloha network, revealing the bi-stability property [45], [46]. Based on the analysis of AoI evolution traces, we derive the expressions of PAoI for each group of the network and the global mean PAoI of the heterogeneous Aloha network.
- *Individual group PAoI optimization:* When only one single group is age-sensitive, we obtain its optimal setting of transmission probability given the transmission probabilities and the scale of other groups. Simulations verify our results and reveal the impact of PAoI optimization of one group on PAoI of other groups.

- *Global mean PAoI optimization:* Based on the Particle Swarm Optimization (PSO) [47], we propose a PAoI optimization algorithm for global PAoI, where the bistable behavior of nodes is considered in algorithm. The algorithm can efficiently converge and obtain the optimal access parameters for each group with different scales and input rates.

The organization of our paper is as follows. In Section II, we obtain the network steady-state point equation based on the Markov chains and derive the expression of PAoI in heterogeneous Aloha networks. In Section III, we give the optimal channel access probability for single-group PAoI optimization, and the results are verified by simulations. The network-wide PAoI optimization is solved in Section IV. Summarizing findings are concluded in Section V.

II. SYSTEM MODEL AND PRELIMINARY ANALYSIS

A. SYSTEM MODEL

Consider a heterogeneous network containing M applications, and the i^{th} group contains $n^{(i)}$ homogeneous sensors, $i = 1, 2, \dots, M$. For illustration, we present Fig. 2 as an example of heterogeneous network having four groups, i.e., $M = 4$. Time is divided into time slots and we assume that all the sensors are synchronized to initiate transmission at the start of each time slot. Each packet transmission takes up a single time slot and the source keeps transmitting the packet over a noiseless channel until acknowledgment (ACK/NACK) message is received, where the ACK/NACK transmission from the destination is error-free and instantaneous [21]. All the sensors from different groups share a common wireless channel and each packet can be successfully transmitted only if there is no concurrent transmission from other sensors.

The Bernoulli packet arrival model is assumed in this work, i.e., the packets arrival of each sensor in the i^{th} group following a Bernoulli process with probability $\lambda^{(i)} \in (0, 1]$. Each sensor is equipped with a buffer of size one. If the buffer is non-empty, the sensor will transmit the packet at the beginning of each time slot with probability $q^{(i)} \in (0, 1]$. The Last-Come-First-Served (LCFS) queue discipline is considered, i.e., the newly arrived packet of the sensor with a non-empty buffer will replace the head-of-line packet.

B. STEADY-STATE POINTS

Let $p^{(i)}$ denote the successful transmission probability of sensors in the i^{th} group. The packet is successfully transmitted if and only if the other sensors have an empty buffer, or have a packet but choose to stay idle. Accordingly, $p^{(i)}$, can be expressed as

$$p^{(i)} = \left(1 - \rho^{(i)} + \rho^{(i)} \left(1 - q^{(i)}\right)\right)^{(n^{(i)}-1)} \cdot \sum_{m=1, m \neq i}^M \left(1 - \rho^{(m)} + \rho^{(m)} \left(1 - q^{(i)}\right)\right)^{n^{(m)}}, \quad (1)$$

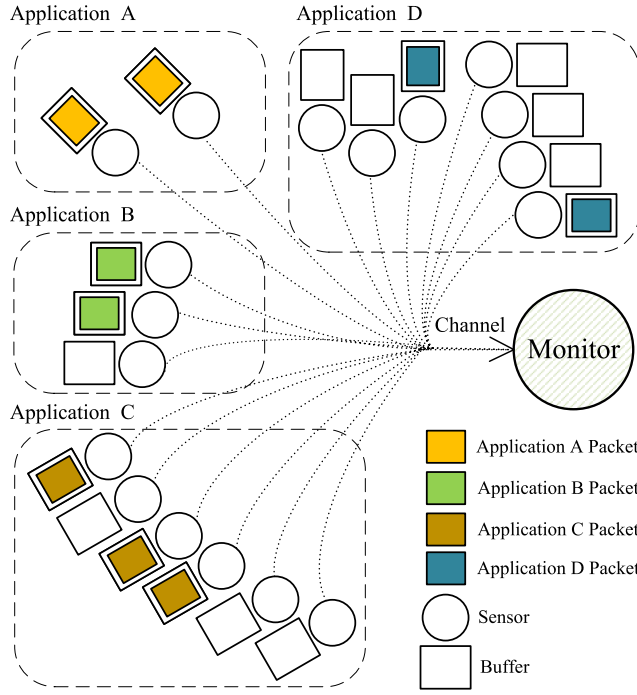


FIGURE 2. A heterogeneous network with multiple applications, $M = 4$ with $n^{(1)} = 2$, $n^{(2)} = 3$, $n^{(3)} = 6$ and $n^{(4)} = 7$.

where $i = 1, 2, \dots, M$ and the offered load is given by [48], [49] as

$$\rho^{(i)} = \frac{\lambda^{(i)}}{\lambda^{(i)} + q^{(i)}p}. \quad (2)$$

Note that all the sensors from different groups share a common channel, and the channel state is identical to all the sensors. Therefore, the successful transmission probability of sensors from different groups is the same that $p^{(i)} = p$. By applying $n - 1 \approx n$ and $(1 - x)^n \approx \exp(-nx)$ for a large n and $0 < x < 1$, we have

$$p \approx \exp\left(-\sum_{m=1}^M \frac{n^{(m)}\lambda^{(m)}q^{(m)}}{\lambda^{(m)} + q^{(m)}p}\right). \quad (3)$$

For illustration, we let $f(p) = \exp(-\sum_{m=1}^M \frac{n^{(m)}\lambda^{(m)}q^{(m)}}{\lambda^{(m)} + q^{(m)}p}) - p$ and $f(p) = 0$ has the same roots as those of (3). Numerical results are presented in Fig. 3. It reveals that (3) has either one root p_L or three roots $0 < p_A < p_S < p_L < 1$, where p_L is the desired steady-state point, p_A is the undesired steady-state point, and p_S is the unstable point [46]. Accordingly, the network has either one steady-state point p_L or two steady-state points with $p_A < p_L$, which is consistent with many studies in slotted Aloha networks [46], [50]. It can be seen from Fig. 3 that as the channel access probability increases, the number of steady-state points may vary from one to two, and the value of undesired steady-state point p_A is far lower than the desired steady-state point p_L .

Let $\mathbf{n} = (n^{(1)}, \dots, n^{(M)})$, $\mathbf{q} = (q^{(1)}, \dots, q^{(M)})$ and $\boldsymbol{\lambda} = (\lambda^{(1)}, \dots, \lambda^{(M)})$ denote the node number vector, the

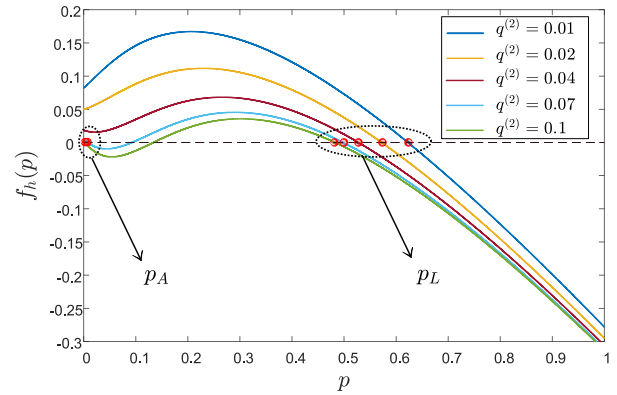


FIGURE 3. Roots of (3). The intersection points of the solid line and the dashed line represent the roots. $M = 2$, $n^{(1)} = n^{(2)} = 50$, $\lambda^{(1)} = \lambda^{(2)} = 0.004$ and $q^{(1)} = 0.05$.

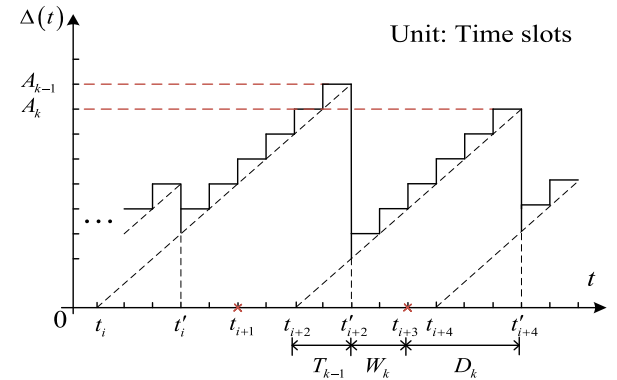


FIGURE 4. Age of information evolution traces.

channel access probability vector, and the input rate vector, respectively. According to (3), the number of roots of (3) in terms of p is closely determined by \mathbf{n} , \mathbf{q} and $\boldsymbol{\lambda}$. Depending on the number of steady-state points, we define the bi-stable region \mathcal{B} and mono-stable region \mathcal{M} below

- *Bi-stable region* $\mathcal{B} = \{(\mathbf{n}, \mathbf{q}, \boldsymbol{\lambda}) |$ the network has two different steady-state points p_A and $p_L\}$.
- *Mono-stable region* $\mathcal{M} = \bar{\mathcal{B}}$, in which the network has only one steady-state point p_L .

Note that the bi-stable behavior of Aloha network has long been observed, that is, in the bi-stable region, there is a potential risk for the network to transition from the desired steady-state point p_L to the undesired steady-state point p_A , on which the performance will be intolerably poor as $p_A \ll p_L$.

C. PEAK AGE OF INFORMATION

The primary focus of this paper is to analyze the network's performance in terms of the PAoI, which is defined as the maximum value of age of information achieved just before an update is received [12]. Fig. 4 illustrates an example of the evolution traces of AoI, where t_i denotes the arrival time of the i^{th} packet and t'_i denotes the successful transmission time of the i^{th} packet, $i \in \{1, 2, \dots\}$. When the buffer size is one, the node only retains the latest packet. For example, at times t'_{i+2} and t'_{i+4} , when a new packet is received by the node, the

old packet (generated at times t'_{i+1} and t'_{i+3}) in the buffer will be discarded. The node's AoI continuously increases over time until a packet is successfully transmitted, such as the instances at t'_{i+2} and t'_{i+4} . Whenever a packet is successfully transmitted, there will be a corresponding PAoI, indicating the maximum AoI reached before successful transmission. Since only successfully transmitted data packets contribute to age performance, we use the subscript k to denote these informative packets [51], [52]. It can be observed from Fig. 4 that the PAoI consists of three parts $A_k = T_{k-1} + W_k + D_k$, where

- T_k represents the service time of the k^{th} informative packet, which is the duration from the arrival of the k^{th} packet to its successful transmission.
- W_k represents the idle period, i.e., the time interval from the successful transmission of the $k - 1^{\text{th}}$ packet until the arrival of a new one.
- D_k represents the access delay, which is the duration from the first packet's arrival after the $k - 1^{\text{th}}$ packet transmission until the successful transmission of the next informative packet.

Since T_k , W_k , and D_k are independent identical distribution (i.i.d.) random variables, the subscript k is dropped in the following analysis.

Let us start by deriving the PAoI for a single group $A^{(i)}$ in heterogeneous Aloha networks. Since the departure of the previously transmitted $i - 1^{\text{th}}$ packet and the arrival of a new packet can coincide in time, and the packet arrival follows the Bernoulli process, we have

$$E[W] = \frac{1}{\lambda^{(i)}} - 1. \quad (4)$$

Existing work on the Aloha network has provided insights into the average access delay and revealed that [50]

$$E[D] = \frac{1}{q^{(i)} p}. \quad (5)$$

To derive the service time T , we examine the condition probability between the service time T and the access delay D . In particular, based on the [50, eq. (1)], the probability mass function of D can be obtained as

$$P\{D = d\} = \begin{cases} q^{(i)} p, & d = 1, \\ (1 - q^{(i)} p)^{d-1} q^{(i)} p, & d \geq 2. \end{cases} \quad (6)$$

Given the access delay D , the service time has $T \leq D$ and let the service time $T = t$ and the access delay $D = d$, the conditional probability denoted as $P\{T = t | D = d\}$, can be obtained as

$$P\{T = t | D = d\} = \begin{cases} (1 - \lambda^{(i)})^{t-1}, & t = d, \\ \lambda^{(i)} (1 - \lambda^{(i)})^{t-1}, & 1 \leq t < d, \end{cases} \quad (7)$$

where $t, d \in \{1, 2, \dots\}$. By combining (6) and (7), the probability mass function of the service time can be derived as

$$\begin{aligned} P\{T = t\} &= \sum_{d=1}^{+\infty} P\{T = t | D = d\} P\{D = d\} \\ &= \left((1 - \lambda^{(i)}) (1 - q^{(i)} p) \right)^{t-1} \left(q^{(i)} p + \lambda^{(i)} (1 - q^{(i)} p) \right). \end{aligned} \quad (8)$$

The probability generating function of T can then be written as

$$G_T(z) = \sum_{t=1}^{+\infty} P\{T = t\} z^t = \frac{(pq^{(i)}(\lambda^{(i)} - 1) - \lambda^{(i)})z}{(\lambda^{(i)} - 1)z(pq^{(i)} - 1) - 1}, \quad (9)$$

with which the average service time can be calculated as

$$E[T] = G'_T(1) = \frac{1}{pq^{(i)} + (1 - pq^{(i)})\lambda^{(i)}}. \quad (10)$$

Finally, the PAoI for a single group $A^{(i)}$ is derived as follow by combing (4), (5) and (10)

$$A^{(i)} = \frac{1}{pq^{(i)}} + \frac{1}{pq^{(i)} + (1 - pq^{(i)})\lambda^{(i)}} + \frac{1}{\lambda^{(i)}} - 1, \quad (11)$$

where the successful transmission probability p is given in (3). Furthermore, the global mean PAoI A , i.e., the mean PAoI of all the sensors from different groups, can be defined as

$$A \triangleq \frac{\sum_{i=1}^M n^{(i)} A^{(i)}}{\sum_{i=1}^M n^{(i)}}. \quad (12)$$

D. OPTIMIZATION PROBLEM

The main goal of our paper is to minimize the PAoI through the optimal configuration of the channel access probability. Specifically, we focus on two specific optimization problems in our study.

The first one is the individual group PAoI optimization problem, where only the group i is age-sensitive. Accordingly, given the backoff parameter settings of all other groups, group i aims at optimizing its PAoI $A^{(i)}$ by tuning the channel access probability¹, i.e.,

$$A^{(i)*} = \min_{0 < q^{(i)} \leq 1} A^{(i)}. \quad (13)$$

The second problem is the global PAoI optimization problem, where all the groups are age-sensitive and we aim at minimizing the global PAoI A via optimally tuning the channel access probability vector \mathbf{q} . According to (12), the optimization problem can be defined as

$$A^* = \min_{\mathbf{0} < \mathbf{q} \leq \mathbf{1}} A. \quad (14)$$

In the following Section III, we focus on the individual group PAoI optimization problem, and the global PAoI optimization will be solved in Section IV.

¹The probability of each device accessing the channel during random access procedure in LTE networks is often referred to as the Access Class Barring (ACB) factor [53].

III. INDIVIDUAL GROUP PAOI OPTIMIZATION

A. OPTIMIZATION ANALYSIS

Let us first consider the individual group PAOI optimization in (13). The following proposition gives the optimal channel access probability $q^{(i)*}$ when the network is operating at the desired steady-state point that $p = p_L$.

Proposition 1: With $p = p_L$, the optimal access probability for minimizing $A^{(i)}$ is given by

$$q^{(i)*}|_{p=p_L} = \begin{cases} q_{opt}^{(i)}, & \text{if } n^{(i)} > n_{th}, \\ 1, & \text{otherwise,} \end{cases} \quad (15)$$

in which n_{th} is given by

$$n_{th} = \left(1 + \frac{p_1}{\lambda^{(i)}}\right) \left(1 - \sum_{m=1, m \neq i}^M \frac{n^{(m)} \lambda^{(m)} q^{(m)2} p|_{q^{(i)}=1}}{\left(\lambda^{(m)} + q^{(m)} p|_{q^{(i)}=1}\right)^2}\right), \quad (16)$$

and $q_{opt}^{(i)}$ is given by

$$q_{opt}^{(i)} = \frac{\lambda^{(i)} \left(1 - \sum_{m=1, m \neq i}^M \frac{n^{(m)} \lambda^{(m)} q^{(m)2} p_*}{\left(\lambda^{(m)} + q^{(m)} p_*\right)^2}\right)}{n^{(i)} \lambda^{(i)} - p_* \left(1 - \sum_{m=1, m \neq i}^M \frac{n^{(m)} \lambda^{(m)} q^{(m)2} p_*}{\left(\lambda^{(m)} + q^{(m)} p_*\right)^2}\right)}, \quad (17)$$

where p_* is the non-zero root of the following equation

$$p_* = \exp \left(-1 - \sum_{m=1, m \neq i}^M \frac{n^{(m)} \lambda^{(m)} q^{(m)2}}{\left(\lambda^{(m)} + q^{(m)} p_*\right)^2} \right). \quad (18)$$

Proof: See Appendix-A. ■

However, as Fig. 3 depicted, the network may not operate at the desired steady-state point since the network may deviate from the desired steady-state point p_L and shift to the undesired steady-state point p_A when the packet arrival rate is low. When the network remains in the bi-stable region and operates at p_A , the network performance will deteriorate sharply. Therefore, the channel access probability should be properly designed to ensure the network stays in the mono-stable region and operates at p_L . Regarding this, the following proposition presents the optimal channel access probability $q^{(i)*}$ for PAOI minimization.

Proposition 2: The optimal channel access probability $q^{(i)*}$ for PAOI $A^{(i)}$ minimization is given by

$$q^{(i)*} = \min \left\{ q_B^{(i)}, q^{(i)*}|_{p=p_L} \right\}, \quad (19)$$

where $q_B^{(i)} = \min \{q^{(i)} | (\mathbf{n}, \mathbf{q}, \boldsymbol{\lambda}) \in \mathcal{B}\}$ and $q^{(i)*}|_{p=p_L}$ is given by (15).

Proof: See Appendix-B. ■

Fig. 5 presents the optimal access probability $q^{(i)*}$, for minimizing PAOI $A^{(i)}$, as a function of the arrival rate $\lambda^{(i)}$ with two branches $q_B^{(i)}$ and $q^{(i)*}|_{p=p_L}$. The mono-stable region and the bi-stable region of network are also shown in Fig. 5. It can be observed that when the arrival rate is low, we have $q^{(i)*}|_{p=p_L} > q_B^{(i)}$, indicating that if the access probability q is set to $q^{(i)*}|_{p=p_L}$, the network will fall in bi-stable region and the network operates at undesired steady-state point $p = p_A$ instead of $p = p_L$. To avoid this situation, the optimal

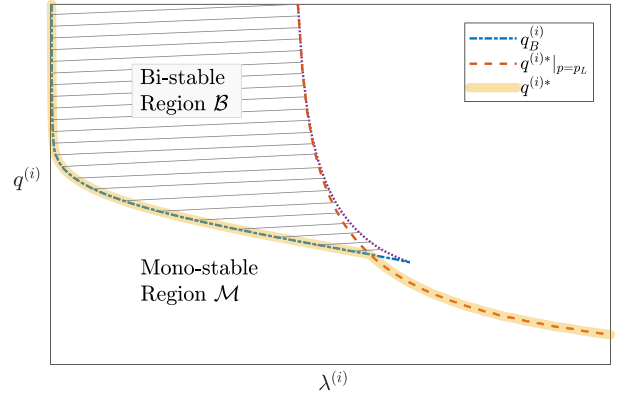


FIGURE 5. Graphic illustration of the Bi-stable region \mathcal{B} , Mono-stable region \mathcal{M} and optimal channel access probability.

access probability is the region boundary $q_B^{(i)}$. Conversely, when the arrival rate is high, the optimal access probability is $q^{(i)*}|_{p=p_L}$ as given in (15). Since we have $q^{(i)*}|_{p=p_L} < q_B^{(i)}$, it enables the network to remain in the mono-stable region and operate at p_L when the access probability is set to $q^{(i)*}|_{p=p_L}$.

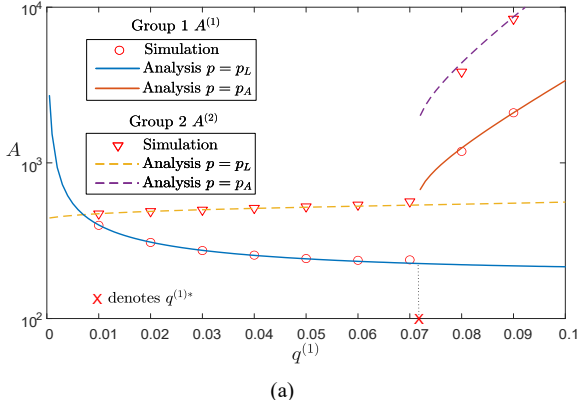
B. SIMULATION RESULTS

In this subsection, we present the simulation results to verify the aforementioned analysis. In this paper, we employed MATLAB to implement the simulation program. We consider a heterogeneous network with two groups, $M = 2$, where group 1 is age-sensitive. The number of sensors are $n^{(1)} = n^{(2)} = 50$.

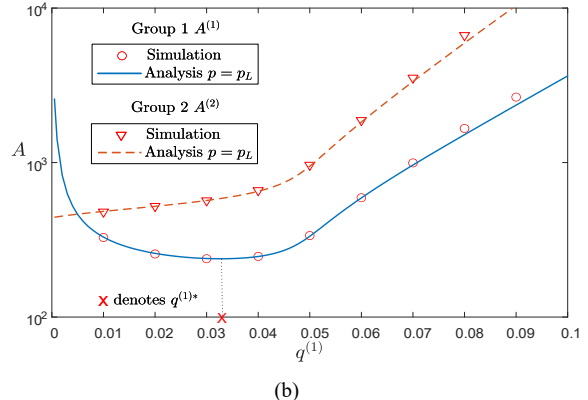
Fig. 6 illustrates how the PAOI $A^{(1)}$ and $A^{(2)}$ varies with the access probability $q^{(1)}$ with the traffic arrival rates are $\lambda^{(1)} = 0.006$ or 0.01 , $\lambda^{(2)} = 0.003$. From Fig. 6 (a), it can be observed that when $\lambda^{(1)}$ is low, tuning the channel access probability $q^{(1)}$ can assist group 1 in achieving a lower PAOI. The interference caused by tuning $q^{(1)}$ to the PAOI of group 2 is negligible when the network remains in the mono-stable region. The optimal channel access probability $q^{(1)*}$ is the boundary value $q_B^{(1)}$ between the mono-stable region and bi-stable region, and the excessive $q^{(1)}$ will lead to worse performance with the undesired steady-state point $p = p_A$.

On the other hand, Fig. 6 (b) shows that when the packet arrival rate $\lambda^{(1)}$ is high, tuning the channel access probability $q^{(1)}$ has a significant impact on the PAOI performance of group 2. The optimal channel access probability is $q^{(1)*}|_{p=p_L}$ as given in (15). While the network always stays in the mono-stable region and avoid operating at the undesired steady-state point $p = p_A$, excessive channel access probability $q^{(1)}$ lead to a significant increase in PAOI for both group 1 and 2, indicating a higher frequency of collisions in the network and resulting in low channel utilization and worse PAOI performances for all the groups.

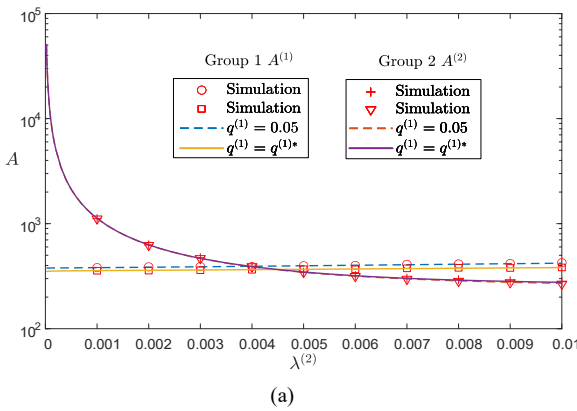
Then we investigate the performance with different packet arrival rates after the optimization of group 1. Fig. 7 shows the PAOI $A^{(1)}$ and $A^{(2)}$ for different packet arrival rates



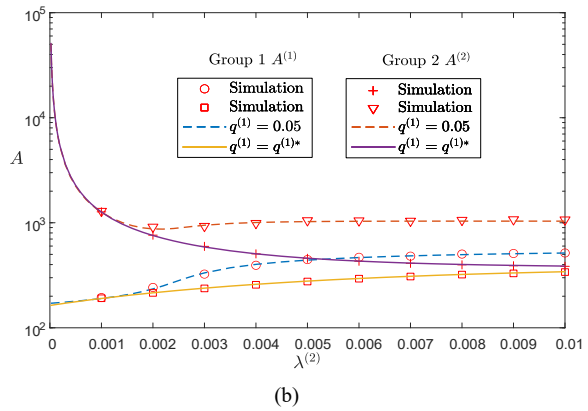
(a)



(b)

FIGURE 6. PAoI $A^{(1)}$ and $A^{(2)}$ versus the channel access probability $q^{(1)}$, $M = 2$, $n^{(1)} = n^{(2)} = 50$, $\lambda^{(2)} = 0.003$ and $q^{(2)} = 0.02$. (a). $\lambda^{(1)} = 0.006$. (b). $\lambda^{(1)} = 0.01$.

(a)



(b)

FIGURE 7. PAoI $A^{(1)}$ and $A^{(2)}$ versus the packet arrival rate $\lambda^{(2)}$, $M = 2$, $n^{(1)} = n^{(2)} = 50$, $q^{(2)} = 0.02$. (a). $\lambda^{(1)} = 0.003$. (b). $\lambda^{(1)} = 0.01$.

after optimization of group 1. As the packet arrival rate of group 2 $\lambda^{(2)}$ increases, the channel contention becomes more competitive, making it harder for group 1 to successfully transmit packets, increasing PAoI of group 1. To prevent the rapid growth of PAoI $A^{(1)}$, group 1 optimized its channel access probability with $q^{(1)} = q^{(1)*}$. From Fig. 7 (a), we can see that when the packet arrival rate $\lambda^{(1)}$ is low, the PAoI $A^{(1)}$ maintains a certain level and only increases slightly with the increase of the group 2's packet arrival rate $\lambda^{(2)}$ after optimization. Comparing the fixed setting $q^{(1)} = 0.05$ and the optimization $q^{(1)} = q^{(1)*}$, it can be observed that the optimization of group 1 has little effect on the PAoI performance of group 2.

On the other hand, it can be seen from Fig. 7 (b) that when the packet arrival rate $\lambda^{(1)}$ is high, though the PAoI $A^{(1)}$ with $q^{(1)} = q^{(1)*}$ increases with $\lambda^{(2)}$, the optimization can prevent the rapid growth of PAoI $A^{(1)}$ by comparing it with the fixed setting $q^{(1)} = 0.05$. Moreover, the optimization of group 1 also decreases the PAoI of group 2 $A^{(2)}$ especially when the arrival rate $\lambda^{(2)}$ is high. This is because the optimization of group 1 properly tunes the channel access probability to avoid collisions as much as possible, leading to a higher successful transmission probability for all groups in the network.

IV. GLOBAL MEAN PAOI OPTIMIZATION

In this section, we consider the global mean PAoI optimization problem, that is, all groups collaboratively tune the channel access probability vector q for minimizing the global mean PAoI A . Note that the optimal access probability of group i , $q^{(i)*}$, has been obtained in (19) given the backoff parameter settings of other groups, i.e., $q^{(j)*}, j \in \{1, 2, \dots, M\}/i$, where M is the number of groups in the heterogeneous Aloha networks. Intuitively, iterative algorithms might be used for iteratively calculating the optimal channel access probability of each group one after another according to (19) until $q^* = (q^{(1)*}, \dots, q^{(M)*})$ converges. However, due to the implicit nature of equation (19) and the well-known bi-stable property of the Aloha network, the optimization results will be highly sensitive to the initial access probability q of other groups and the sequence in which each group undergoes individual optimization. Consequently, solving the global PAoI optimization problem iteratively through individual optimization is not feasible.

It should be pointed out that the global mean PAoI optimization problem in (14) is a constrained multivariate optimization with an implicit objective function, which is NP-hard. To cope with this problem, we leverage the particle swarm optimization (PSO) approach to obtain the optimal

channel access probability vector for the global mean PAoI minimization with the bi-stable characteristic of Aloha being considered.

A. PSO-BASED GLOBAL MEAN PAOI OPTIMIZATION ALGORITHM

PSO is a stochastic optimization approach that draws inspiration from the collective behavior observed in a flock of birds. [54], [55], [56], [57]. The problem is solved by cooperation and information sharing among the particles. The position of each particle is a possible solution for the optimization problem and each position corresponds to a fitness value to evaluate the solution. The particles are grouped into a swarm and they will update their velocity and position in each iteration until the termination condition is satisfied.

Let us consider K particles with each particle $k \in \{1, 2, \dots, K\}$ corresponding to its position vector \mathbf{q}_k and velocity vector \mathbf{v}_k . Each particle with position \mathbf{q}_k can calculate its PAoI according to (12) to evaluate the position. For each iteration, each particle will update its velocity and position to explore the optimal position. Specifically, the k^{th} particle in the i^{th} iteration will update its velocity and position according to the following formula [58]

$$\begin{cases} \mathbf{v}_k^{(i+1)} = \omega^{(i)} \cdot \mathbf{v}_k^{(i)} + c_1 r_{1,k}^{(i)} \cdot (\mathbf{b}_k^{(i)} - \mathbf{q}_k^{(i)}) \\ + c_2 r_{2,k}^{(i)} \cdot (\mathbf{d}^{(i)} - \mathbf{q}_k^{(i)}), \\ \mathbf{q}_k^{(i+1)} = \mathbf{v}_k^{(i+1)} + \mathbf{q}_k^{(i)}, \end{cases} \quad (20)$$

where c_1 and c_2 are the learning weight, $r_{1,k}^{(i)}$ and $r_{2,k}^{(i)}$ are the random value uniformly generated from the range $[0, 1]$, $\mathbf{b}_k^{(i)}$ denotes the best-experienced position of the particle itself and $\mathbf{d}^{(i)}$ denotes the best-experienced position among all particles, which are determined by [58]

$$\begin{cases} \mathbf{b}_k^{(i)} = \underset{\mathbf{q}_k^{(1)}, \mathbf{q}_k^{(2)}, \dots, \mathbf{q}_k^{(i)}}{\operatorname{argmin}} A, \\ \mathbf{d}^{(i)} = \underset{\mathbf{b}_1^{(i)}, \mathbf{b}_2^{(i)}, \dots, \mathbf{b}_K^{(i)}}{\operatorname{argmin}} A, \end{cases} \quad (21)$$

with the corresponding PAoI $A_k^{(i)} = A|_{\mathbf{q}=\mathbf{b}_k^{(i)}}$, $A_d^{(i)} = A|_{\mathbf{q}=\mathbf{d}^{(i)}}$ and $\omega^{(i)}$ is the inertia weight which is decreased monotonously with iterations number and is given by [58]

$$\omega^{(i)} = \omega_{\min} + \frac{(\omega_{\max} - \omega_{\min}) \cdot i}{I_{\max}}, \quad (22)$$

where I_{\max} is the upper-bound of the number of iterations, ω_{\min} and ω_{\max} are the minimum and maximum inertia weight.

The detailed implementation of our PSO algorithm is described in Algorithm 1. For each iteration, the particles will update their velocity and position (i.e., channel access probability vector) towards the minimization of global mean PAoI.

To make it appropriate for Aloha network and further improve the performance of PSO algorithm, we revise the

Algorithm 1 PSO Algorithm for Global Mean PAoI Minimization

Input: Network parameters $n^{(m)}$, $\lambda^{(m)}$, $m = 1, 2, \dots, M$, and algorithm setting K , c_1 , c_2 , v_{\min} , v_{\max} , \mathbf{q}_{\min} , \mathbf{q}_{\max} , ω_{\min} , ω_{\max} , I_{\max} .

Output: Optimal channel access probability $\mathbf{d}^{(I_{\max})} = [q^{(1)}, q^{(2)}, \dots, q^{(M)}]$ and minimum global PAoI $A_d^{(I_{\max})}$.

```

1: for each particle  $k = 1$  to  $K$  do
2:   Initialize position  $\mathbf{q}_k^{(1)}$  and velocity  $\mathbf{v}_k^{(1)}$ 
3:    $\mathbf{b}_k^{(1)} = \mathbf{q}_k^{(1)}$ 
4:   Calculate the PAoI  $A_k^{(1)}$  according to (12)
5: end for
6: Initialize  $[\mathbf{d}^{(1)}, A_d^{(1)}]$  according to (21) and (12)
7: Set iteration indicator  $i = 1$ 
8: for Iteration  $i < I_{\max}$  do
9:   for each particle  $k = 1$  to  $K$  do
10:    Update velocity  $\mathbf{v}_k^{(i+1)}$  according to (20)
11:     $\mathbf{v}_k^{(i+1)} = \max(\mathbf{v}_k^{(i+1)}, v_{\max})$ 
12:     $\mathbf{v}_k^{(i+1)} = \min(\mathbf{v}_k^{(i+1)}, v_{\min})$ 
13:    Update position  $\mathbf{q}_k^{(i+1)} = \mathbf{v}_k^{(i+1)} + \mathbf{q}_k^{(i)}$ 
14:     $\mathbf{q}_k^{(i+1)} = \max(\mathbf{q}_k^{(i+1)}, \mathbf{q}_{\max})$ 
15:     $\mathbf{q}_k^{(i+1)} = \min(\mathbf{q}_k^{(i+1)}, \mathbf{q}_{\min})$ 
16:    Calculate the steady-state point according to (3)
17:    if the undesired steady-state point  $p_A$  exists then
18:      Let  $p = p_A$ 
19:    else
20:      Let  $p = p_L$ 
21:    end if
22:    Calculate the PAoI according to (12)
23:    Update  $[\mathbf{b}_k^{(i+1)}, A_k^{(i+1)}]$  according to (21) and (12)
24:  end for
25:  Update  $[\mathbf{d}^{(i+1)}, A_d^{(i+1)}]$  according to (21) and (12)
26:  Update  $\omega^{(i+1)}$  according to (22)
27:   $i = i + 1$ 
28: end for

```

conventional PSO algorithm by introducing the bi-stable behavior of Aloha into consideration. Specifically, for the global PAoI calculation from line 17 to line 21, when each particle calculates its global PAoI, it will first determine the number of steady-state points in (3), i.e., if the undesired steady-state point p_A exists, then the network is in the bi-stable region \mathcal{B} ; otherwise, the network is in the mono-stable region \mathcal{M} . Recall that in \mathcal{B} , the network suffers the potential risk of transitioning from the desired point p_L to the undesired one p_A , on which the network performance becomes intolerably poor. To avoid this risk, the proposed PSO algorithm assumes $p = p_A$ if p_A exists, leading to a high PAoI that holds back the particle exploration towards \mathcal{B} .

B. COMPLEXITY ANALYSIS

In this subsection, we analyze the complexity of Algorithm 1. In addition to the initialization from line 1 to line 7, there are three nested loops in Algorithm 1. The

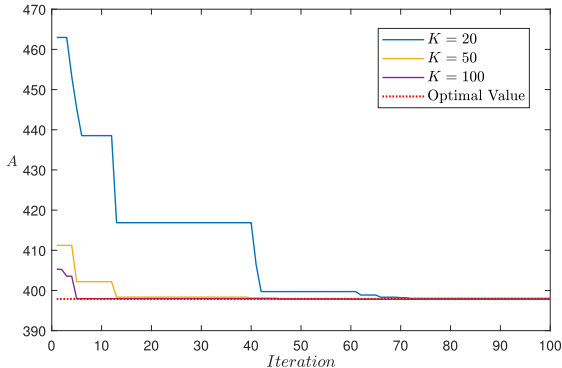


FIGURE 8. Optimal global PAoI A with iteration round i from 1 to 100, $M = 2$, $n^{(1)} = n^{(2)} = 50$, $\lambda^{(1)} = 0.002$ and $\lambda^{(2)} = 0.006$.

outer loop is from line 8 to line 28 and it reflects the number of iterations in the algorithm, which introduce the computation complexity $\mathcal{O}(I_{max})$. The second loop is from line 9 to line 24, which reflects the action of different particles and introduces the computation complexity $\mathcal{O}(K)$. The inner loop is line 23, which is the process of updating the channel access probability of different groups and introducing the computation complexity $\mathcal{O}(M)$. Finally, the computation complexity of Algorithm 1 can be obtained as $\mathcal{O}(I_{max} \cdot K \cdot M)$.

C. CONVERGENCE

In this subsection, we show the iteration process of a heterogeneous network with two groups. The number of sensors $n^{(1)} = n^{(2)} = 50$, and the packer arrival rates are $\lambda^{(1)} = 0.002$ and $\lambda^{(2)} = 0.006$. We use Algorithm 1 to seek the optimal access parameters $q^{(1)}$ and $q^{(2)}$ for minimizing the global PAoI. The Algorithm parameter settings are given in Table I. Fig. 8 shows the optimal global PAoI obtained in each iteration, and the optimal PAoI by ergodic searching is illustrated in the same figure. It can be seen that the algorithm converges and the output is close to the optimal solution of the problem. With a larger number of particles K , the algorithm converges faster. With $K = 20, 50$, or 100 , the algorithm converges to a similar value and has almost the same output.

Fig. 9 illustrates a different view of the convergence. The PAoI with the network steady-state point $p = p_L$ and $p = p_A$ are depicted together, and the particles are marked. We ran our simulation programs on a computer equipped with a single CPU (Intel Core i7-11700, CPU clock 2.50 GHz) and RAM (DDR4, 16G*2, clock 2933MHz). The algorithmic process corresponding to Fig. 9 took a total of 42.63 milliseconds. It can be observed that the particles are spotted at first, shift from the bi-stable region to the mono-stable region gradually, and approach the optimal solution in the feasible region. According to Eq. (20) and (22), the inertia weight will decrease with iteration number i and the particles will converge step by step and get a more accurate output in the later iteration period. Note that despite some

particles remaining in the bi-stable region during the iteration process, the algorithm outputs the unique position of the optimum historically reached by the particles. Therefore, whether the particles are exploring in the bi-stable region or those that had reached the optimum but left by the iteration's end does not affect the algorithm's capability to output the optimal solution.

D. PERFORMANCE EVALUATION

In this subsection, we present the simulation results for the global PAoI optimization in a heterogeneous network with two groups that $M = 2$. The optimal channel access probabilities are obtained by applying Algorithm 1 with the number of particles $K = 100$, and the same algorithm parameters as listed in Table 1.

Fig. 10 and Fig. 11 present the network performance with the arrival rate of group 2 $\lambda^{(2)}$ varying. Specifically, Fig. 10 (a) demonstrates how the optimal access probability of two groups $q^{(1)*}, q^{(2)*}$ vary with the arrival rate $\lambda^{(2)}$. As $\lambda^{(2)}$ increases, the optimal access probability $q^{(2)*}$ decreases due to the increased number of sensors in group 2, and the access probability must be tuned lower to avoid collisions. The corresponding PAoI for two groups $A^{(1)}, A^{(2)}$ and global PAoI A are illustrated in Fig. 10 (b). It can be observed that the PAoI of group 2 $A^{(2)}$ decreases as $\lambda^{(2)}$ increases, because more fresh packets are available for transmission with higher input rate $\lambda^{(2)}$, even though the access probability $q^{(2)}$ has been tuned lower. On the other hand, with $\lambda^{(2)}$ increases, the optimal access probability of group 1 will increase to strive for more opportunities for successful transmission, and the PAoI $A^{(1)}$ is maintained at a certain level corresponding to its packet arrival rate $\lambda^{(1)} = 0.002$.

The simulation results of network performance with higher packet arrival rate $\lambda^{(1)}$ are depicted in Fig. 11. Fig. 11 (a) presents how the network steady-state point (i.e., the successful transmission probability) varies with the packet arrival rate of group 2 $\lambda^{(2)}$ while $\lambda^{(1)} \in \{0.002, 0.004, 0.006, 0.008\}$. As $\lambda^{(1)}$ or $\lambda^{(2)}$ increases, the network steady-state point decreases particularly when the input rate of another group is small. It is worth noting that with optimal channel access probabilities obtained by PSO Algorithm, the network steady-state point is always greater than or equal to e^{-1} .

Meanwhile, the corresponding minimum global PAoI A is illustrated in Fig. 11 (b). As $\lambda^{(1)}$ increases, the global PAoI decreases only when $\lambda^{(2)}$ is small. When $\lambda^{(1)}$ is fixed, there exists an optimal $\lambda^{(2)}$ that can achieve the minimum A . Furthermore, when $\lambda^{(2)}$ is high, $\lambda^{(1)}$ cannot be too high or too low to achieve the minimum global PAoI. This is because, with more packets arriving in group 1, the network is more congested, and is harder for the sensors in both groups to access the channel and transmit their packets. On the other hand, if $\lambda^{(1)}$ is too low, there are not enough packets in group 1 to transmit, resulting in fairness issue and high global PAoI.

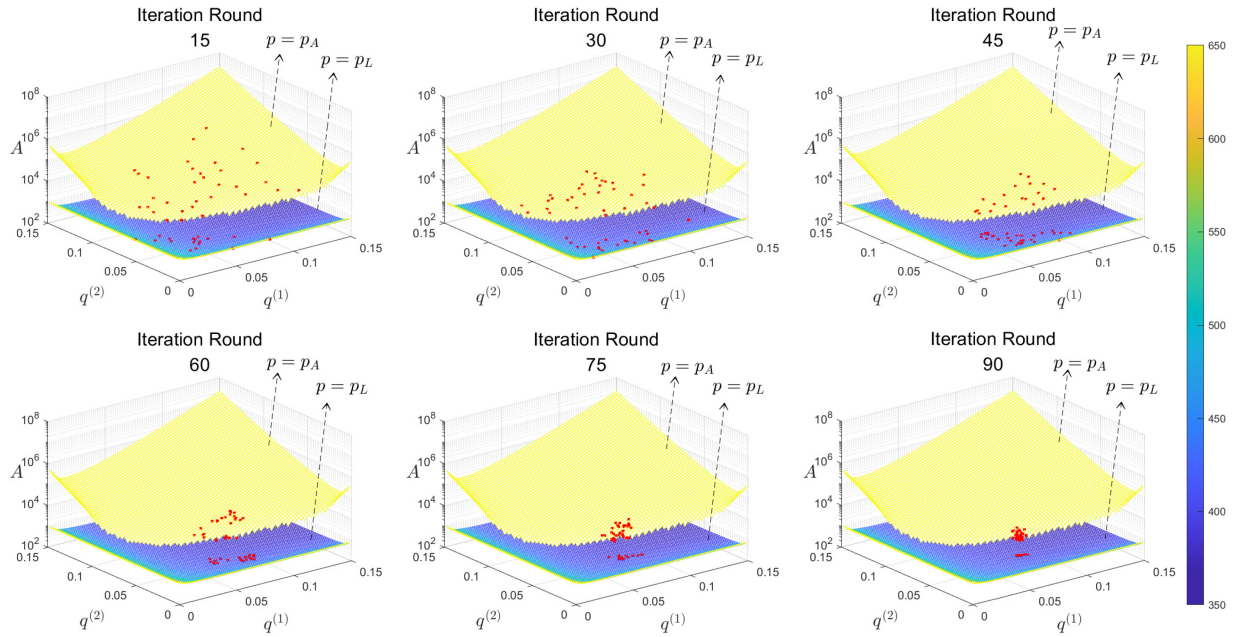


FIGURE 9. Particle positions with iteration round $i = 15, 30, 45, 60, 75, 90$, $M = 2$, $n^{(1)} = n^{(2)} = 50$, $\lambda^{(1)} = 0.002$ and $\lambda^{(2)} = 0.006$.

TABLE 1. PSO algorithm parameter setting.

Parameters	Values
Number of particles K	50
Self control factor c_1	0.003
Group control factor c_2	0.06
Velocity bounds (v_{min}, v_{max})	(-0.002, 0.002)
Position bounds (q_{min}, q_{max})	(0, 0.15)
Inertia bounds ($\omega_{min}, \omega_{max}$)	(0.4, 2)
Maximum iteration I_{max}	100

Fig. 12 and Fig. 13 demonstrate the impact of the number of sensors in two groups $n^{(1)}$ and $n^{(2)}$ on the network performance. Specifically, Fig. 12 (a) displays how the optimal channel access probability of two groups varies with the number of sensors in group 2 $n^{(2)}$. It can be observed that as $n^{(2)}$ increases, the optimal access probability of two groups $q^{(1)*}$ and $q^{(2)*}$ decrease due to increased channel contention resulting from more sensors in the network. When $n^{(2)}$ is increased from 125 to 150, $q^{(2)*}$ decreases significantly because of a shift in the optimal access probability that is similar to Fig. 5 in the single group optimization. Fig. 12 (b) illustrates the corresponding PAoI for two groups $A^{(1)}, A^{(2)}$ and global A , showing that the PAoI of both groups increases with $n^{(2)}$, and the global PAoI A grows approximately linearly. When $n^{(2)} < n^{(1)}$, the PAoI in group 2 is always higher than that $A^{(1)}$ and once $n^{(2)}$ has increased to that $n^{(2)} > n^{(1)}$, the PAoI in group 2 is consistently lower than that of group 1, even though the packet arrival rate $\lambda^{(2)}$ is lower than $\lambda^{(1)}$.

Moreover, Fig. 13 presents the impact of $n^{(1)}$ on the network performance. The network operation point p is

depicted in Fig. 13 (a) and it can be observed that the network steady-state point decreases as $n^{(1)}$ or $n^{(2)}$ increases at first, particularly when the number of sensors in another group is small, and finally will maintain at e^{-1} with optimal access probabilities obtained by PSO Algorithm. Fig. 13 (b) shows the corresponding minimum global PAoI A , revealing that A will increase as the number of sensors $n^{(1)}$ or $n^{(2)}$ increases, and optimal global PAoI increases at a near-linear trend.

In order to demonstrate the difference between the proposed algorithm and the original PSO [56], Table 2 gives the output results of those two algorithms for the problem (14). With the optimal access parameter q obtained by two algorithms, respectively, simulations are conducted to verify the results with a runtime of 10^8 slots. It can be seen that when $\lambda^{(1)}$ is small, the original PSO theoretically obtains a lower PAoI, but this result can not be achieved in simulation due to the bi-stable property of Aloha. That is, the minimum PAoI is achieved at the desired steady-state point p_L in the bi-stable region. Yet, the network drops to the undesired steady-state point p_A , where $p_A \ll p_L$ and the PAoI on p_A is intolerably large and even much higher than the 10^8 time slots. In contrast, our proposed Algorithm 1 takes the bi-stable property into consideration. The simulation results based on the optimal access parameters of Algorithm 1 match the theoretical results and PAoI performance can be guaranteed.

So far, the effectiveness of the proposed algorithm has been validated, which can minimize the global mean PAoI minimization while the bi-stability of Aloha network is considered for avoiding the risk of rapid performance deterioration. The proposed algorithm can be used in massive

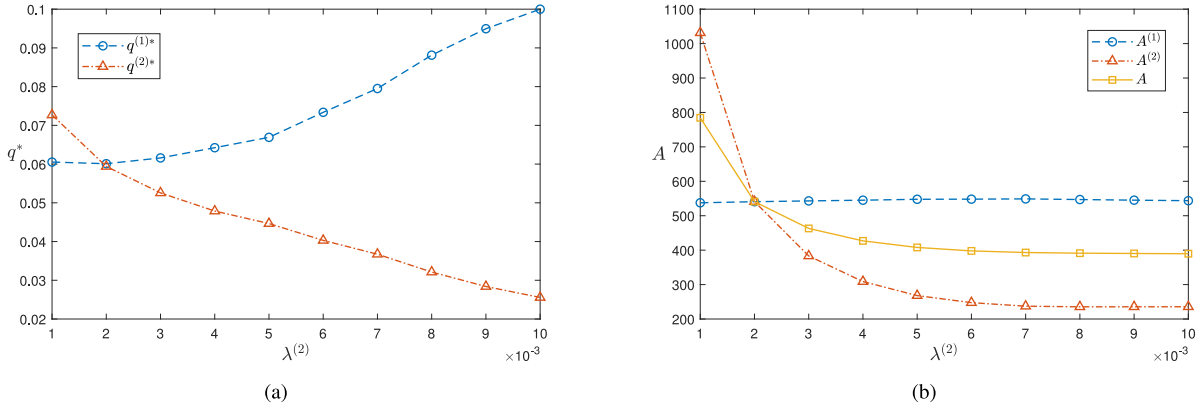


FIGURE 10. Simulation results of (a) optimal access probability $q^{(1)*}$, $q^{(2)*}$ and (b) PAoI $A^{(1)}$, $A^{(2)}$ and global PAoI A versus the packet arrival rate $\lambda^{(2)}$. $M = 2$, $n^{(1)} = n^{(2)} = 50$, $\lambda^{(1)} = 0.002$.

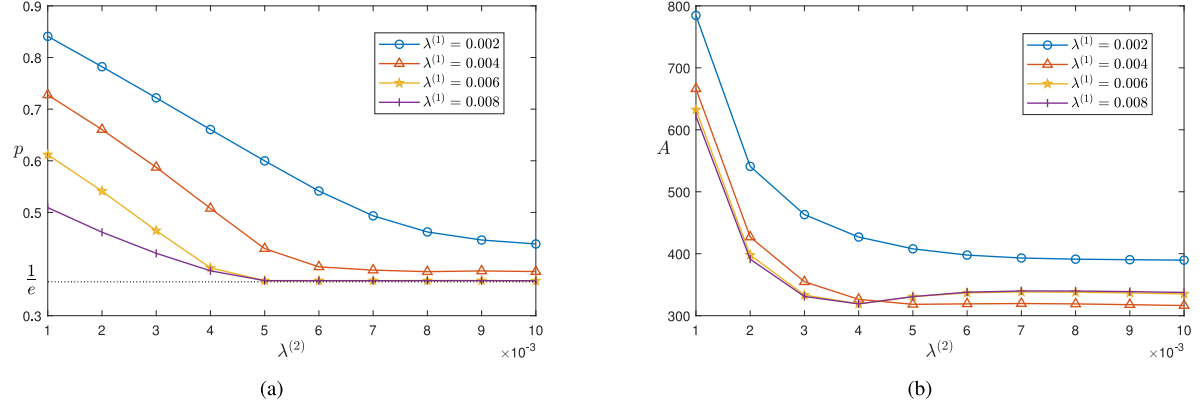


FIGURE 11. Simulation results of (a) steady-state point p and (b) global PAoI A versus the packet arrival rate $\lambda^{(2)}$. $M = 2$, $n^{(1)} = n^{(2)} = 50$, $\lambda^{(1)} = 0.002, 0.004, 0.006, 0.008$.

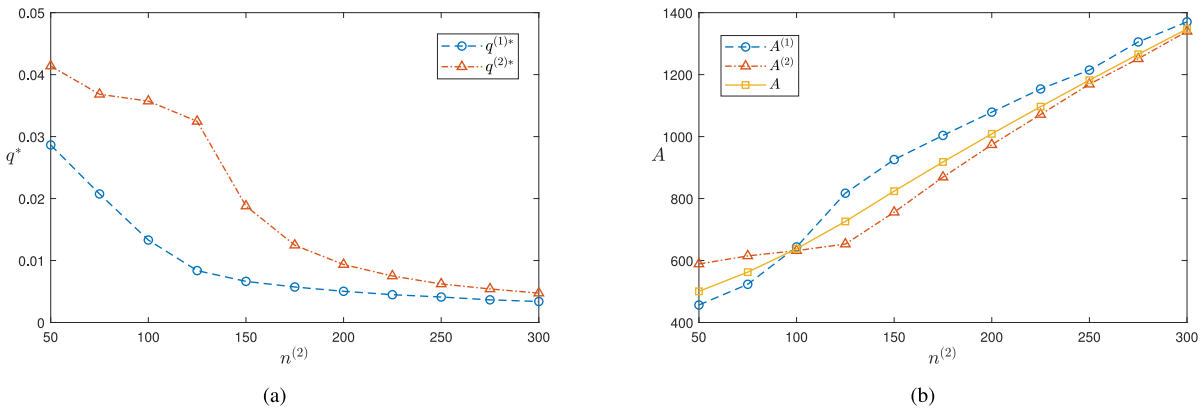
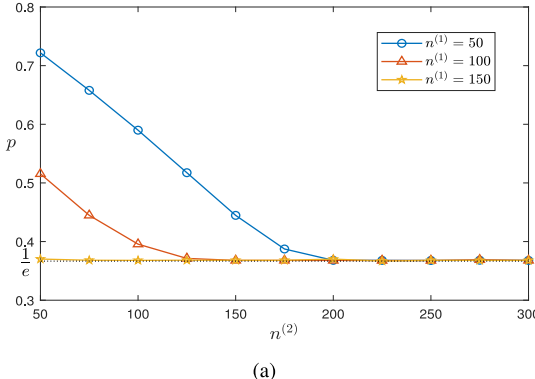


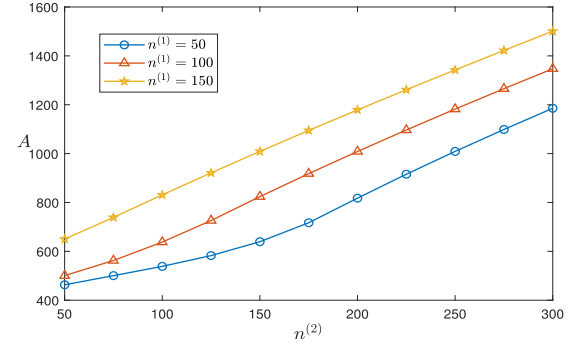
FIGURE 12. Simulation results of (a) optimal access probability $q^{(1)*}$, $q^{(2)*}$ and (b) PAoI $A^{(1)}$, $A^{(2)}$ and global PAoI A versus the number of sensors $n^{(2)}$. $M = 2$, $n^{(1)} = 100$, $\lambda^{(1)} = 0.003$, $\lambda^{(2)} = 0.002$.

random access scenarios with applications which have heterogeneous quality-of-service requirements on information freshness. Examples include: Environmental monitoring,

where the collection of data on climate, soil conditions and pollutant levels can be time-insensitive while fire warning monitoring is time-sensitive.



(a)



(b)

FIGURE 13. Simulation results of (a) steady-state point p and (b) global PAoI A versus the number of sensors $n^{(2)}$. $M = 2$, $\lambda^{(1)} = 0.003$, $\lambda^{(2)} = 0.002$, $n^{(1)} = 50, 100, 150$.

TABLE 2. Theoretical and simulation results of original PSO and proposed algorithm, $M = 2$, $n^{(1)} = n^{(2)} = 50$, $\lambda^{(1)} = \{0.001, 0.003, \dots, 0.011\}$ and $\lambda^{(2)} = 0.006$. The algorithm parameters for both are $K = 100$, $c_1 = 0.003$, $c_2 = 0.06$, $(v_{min}, v_{max}) = (-0.02, 0.02)$, $(q_{min}, q_{max}) = (0, 1)$, $(\omega_{min}, \omega_{max}) = (0.5, 2)$, $I_{max} = 200$.

$\lambda^{(1)}$	Original PSO Algorithm A		Proposed Algorithm A	
	Output	Simulation	Output	Simulation
0.001	586.37	$> 10^8$	632.37	634.61
0.003	306.17	$> 10^8$	333.41	337.93
0.005	330.72	335.98	330.71	334.43
0.007	338.36	338.04	338.36	338.20
0.009	336.70	335.42	336.69	334.94
0.011	333.64	332.39	333.62	331.90

V. CONCLUSION

In this paper, we aim at addressing how to characterize and optimize peak age-of-information performance for heterogeneous Aloha networks, where multiple application groups with different numbers of sensors and packet arrival rates. Specifically, we derive the optimal access probability for single-group PAoI optimization. On the other hand, when all the groups are time-sensitive applications, we propose an algorithm for global PAoI minimization based on the PSO method, which can effectively mitigates the risk of dropping to the undesired network steady-state point with intolerable performance and obtain the optimal access parameters for each of the heterogeneous groups to achieve the minimum global PAoI. Simulations verify our results and reveal that when the packet arrival rates are large, the PAoI optimization of a single group can also improve the PAoI of other groups. When all the groups are time-sensitive applications, our results for global PAoI optimization indicate that the network steady-state point is always no less than e^{-1} , and the minimum global PAoI increases linearly with the network scale.

APPENDIX

A. PROOF OF PROPOSITION 1

To minimize the PAoI of its group $A^{(i)}$, we can derive the optimal channel access probability $q^{(i)}$ for the i^{th} group by calculating the first derivative. According to (11), we have

$$\frac{\partial A^{(i)}}{\partial q^{(i)}} = \left(\frac{\partial p}{\partial q^{(i)}} q^{(i)} + p \right) \left(\frac{-1}{(q^{(i)} p)^2} - \frac{1 - \lambda^{(i)}}{(q^{(i)} p (1 - \lambda^{(i)}) + \lambda^{(i)})^2} \right). \quad (23)$$

According to (3), we have

$$\frac{\partial p}{\partial q^{(i)}} = \frac{n^{(i)} \lambda^{(i)} p}{(\lambda^{(i)} + p q^{(i)})^2 \left(-1 + p \sum_{m=1}^M \frac{n^{(m)} \lambda^{(m)} q^{(m)2}}{(\lambda^{(m)} + p q^{(m)})^2} \right)}. \quad (24)$$

By substituting (24) into (23), we have

$$\lim_{q^{(i)} \rightarrow 0} \frac{\partial A^{(i)}}{\partial q^{(i)}} = -\infty < 0, \quad (25)$$

and (26), shown at the top of the next page where p_1 is the non-zero root of the following equation

$$p_1 = \exp \left(- \sum_{m=1}^M \frac{n^{(m)} \lambda^{(m)} q^{(m)}}{\lambda^{(m)} + p q^{(m)} p_1} \right) \Big|_{q^{(i)}=1}. \quad (27)$$

With the increase of channel access probability $q^{(i)}$, the channel competition becomes more intense and the successful transmission probability p monotonically decreases. According to (24), we have

$$-1 + \sum_{m=1}^M \frac{n^{(m)} \lambda^{(m)} p q^{(m)2}}{(\lambda^{(m)} + p q^{(m)})^2} < 0. \quad (28)$$

Since the network operates at the desired steady-state point p_L , by combining (26)-(28), when

$$n^{(i)} > \left(1 + \frac{p_1}{\lambda^{(i)}} \right) \left(1 - \sum_{m=1, m \neq i}^M \frac{n^{(m)} \lambda^{(m)} q^{(m)2} p_1}{(\lambda^{(m)} + p_1 q^{(m)})^2} \right) \quad (29)$$

holds, we have $\lim_{q^{(i)} \rightarrow 1} \frac{\partial A^{(i)}}{\partial q^{(i)}} > 0$. Then the PAoI $A^{(i)}$ can be optimized in $q \in (0, 1)$. By combining (23) and (24), we can simplify $\frac{\partial A^{(i)}}{\partial q^{(i)}} = 0$ as

$$1 - \frac{n^{(i)} \lambda^{(i)} q^{(i)}}{\lambda^{(i)} + p q^{(i)}} = \sum_{m=1, m \neq i}^M \frac{n^{(m)} \lambda^{(m)} q^{(m)2} p}{(\lambda^{(m)} + p q^{(m)})^2}, \quad (30)$$

based on which the optimal channel access probability in (17) is obtained, where (18) is the desired network steady-state point p_L by substituting (17) into (3). Otherwise, we have $\frac{\partial A^{(i)}}{\partial q^{(i)}} \leq 0$ for $q \in (0, 1]$ and the optimal channel access probability is given by $q^{(i)} = 1$.

$$\lim_{q^{(i)} \rightarrow 1} \frac{\partial A^{(i)}}{\partial q^{(i)}} = \left(\frac{n^{(i)} \lambda^{(i)} p_1}{(\lambda^{(i)} + p_1)^2 \left(-1 + p_1 + \sum_{m=1}^M \frac{n^{(m)} \lambda^{(m)} q^{(m)2}}{(\lambda^{(m)} + p_1 q^{(m)})^2} \right)} \Big|_{q^{(i)}=1} + p_1 \right) \cdot \left(-\frac{1}{p_1^2} - \frac{1 - \lambda^{(i)}}{(p_1(1 - \lambda^{(i)}) + \lambda^{(i)})^2} \right). \quad (26)$$

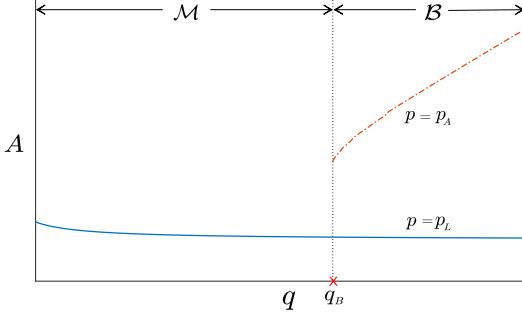


FIGURE 14. PAoI versus the channel access probability.

B. PROOF OF PROPOSITION 2

According to (23) and (24), we can obtain the first derivative $\frac{\partial A^{(i)}}{\partial q^{(i)}}$ when the network stays in the mono-stable region operating at the desired steady-state point $p = p_L$. When the transmission probability $q < q^{(i)*}|_{p=p_L}$, we have $\frac{\partial A^{(i)}}{\partial q^{(i)}} < 0$, implying that the PAoI will decrease as q increases. Fig. 14 depicts the PAoI performance versus the channel access probability, and specifically, the PAoI performance when the network shifts from the mono-stable region to the bi-stable region. We note the access probability at the boundary between the mono-stable region and bi-stable region as $q_B^{(i)}$, i.e.,

$$q_B^{(i)} = \min \left\{ q_B^{(i)} | (\mathbf{n}, \mathbf{q}, \boldsymbol{\lambda}) \in \mathcal{B} \right\}. \quad (31)$$

When the boundary value $q_B^{(i)} \notin (0, 1]$, the network stays in mono-stable region and $q^{(i)*}|_{p=p_L}$ can achieve the minimum PAoI. Otherwise, there have two cases when $q_B^{(i)} \in (0, 1]$:

1) When $q^{(i)*}|_{p=p_L} > q_B^{(i)}$, it indicates that the optimal channel access probability $q^{(i)*}|_{p=p_L}$ is higher than the boundary value, so the network will shift to bi-stable region and the condition $p = p_L$ is not hold anymore if $q = q^{(i)*}|_{p=p_L}$. As the access probability increases, the PAoI decreases in the mono-stable region. If $q^{(i)*}|_{p=p_L}$ is larger than the boundary value $q_B^{(i)}$, the optimal access parameter should be set to $q_B^{(i)}$ to avoid the poor performance that the network shifts to the bi-stable region and operates at $p = p_A$. The optimal channel access probability should be set to $q_B^{(i)}$, i.e.,

$$\arg \min_{q^{(i)}} A^{(i)} \Big|_{q^{(i)*}|_{p=p_L} > q_B^{(i)}} = q_B^{(i)}. \quad (32)$$

2) When $q^{(i)*}|_{p=p_L} \leq q_B^{(i)}$, then the optimal channel access probability $q^{(i)*}|_{p=p_L}$ can ensure that the network operating in \mathcal{M} at the desired steady-state point p_L while achieving the minimum PAoI. The optimal channel access probability should be set to $q^{(i)*}|_{p=p_L}$, i.e.,

$$\arg \min_{q^{(i)}} A^{(i)} \Big|_{q^{(i)*}|_{p=p_L} \leq q_B^{(i)}} = q^{(i)*}|_{p=p_L}. \quad (33)$$

Finally, the optimal access probability for PAoI minimization in (19) can be obtained by combining the above analysis.

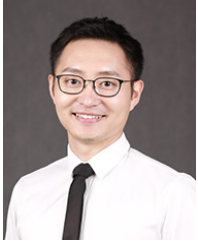
REFERENCES

- [1] Z. Ling, F. Hu, H. Zhang, and Z. Han, “Age-of-information minimization in healthcare IoT using distributionally robust optimization,” *IEEE Internet Things J.*, vol. 9, no. 17, pp. 16154–16167, Sep. 2022.
- [2] X. Wang, C. Chen, J. He, S. Zhu, and X. Guan, “AoI-aware control and communication co-design for industrial IoT systems,” *IEEE Internet Things J.*, vol. 8, no. 10, pp. 8464–8473, May 2021.
- [3] H. Huang, S. Guo, W. Liang, K. Wang, and A. Y. Zomaya, “Green data-collection from geo-distributed IoT networks through low-earth-orbit satellites,” *IEEE Trans. Green Commun. Netw.*, vol. 3, no. 3, pp. 806–816, Sep. 2019.
- [4] M. A. Abd-Elmagid, N. Pappas, and H. S. Dhillon, “On the role of age of information in the Internet of Things,” *IEEE Commun. Mag.*, vol. 57, no. 12, pp. 72–77, Dec. 2019.
- [5] S. B. Baker, W. Xiang, and I. Atkinson, “Internet of Things for smart healthcare: Technologies, challenges, and opportunities,” *IEEE Access*, vol. 5, pp. 26521–26544, 2017.
- [6] L. Lyu, C. Chen, S. Zhu, and X. Guan, “5G enabled codesign of energy-efficient transmission and estimation for industrial IoT systems,” *IEEE Trans. Ind. Inf.*, vol. 14, no. 6, pp. 2690–2704, Jun. 2018.
- [7] X. Xie, H. Wang, and X. Liu, “Scheduling for minimizing the age of information in multisensor multiserver Industrial Internet of Things systems,” *IEEE Trans. Ind. Inf.*, vol. 20, no. 1, pp. 573–582, Jan. 2024.
- [8] C. Guo, X. Wang, L. Liang, and G. Y. Li, “Age of information, latency, and reliability in intelligent vehicular networks,” *IEEE Network*, vol. 37, no. 6, pp. 109–116, Nov. 2023.
- [9] I. Kahraman, A. Kose, M. Koca, and E. Anarim, “Age of information in Internet of Things: A survey,” *IEEE Internet Things J.*, vol. 11, no. 6, pp. 9896–9914, Mar. 2024.
- [10] B. Yu, X. Chen, and Y. Cai, “Age of information for the cellular Internet of Things: Challenges, key techniques, and future trends,” *IEEE Commun. Mag.*, vol. 60, no. 12, pp. 20–26, Dec. 2022.
- [11] S. Kaul, R. Yates, and M. Gruteser, “Real-time status: How often should one update?” in *Proc. IEEE INFOCOM*, 2012, pp. 2731–2735.
- [12] M. Costa, M. Codreanu, and A. Ephremides, “Age of information with packet management,” in *Proc. IEEE Int. Symp. Inf. Theory*, Honolulu, HI, USA, 2014, pp. 1583–1587.
- [13] L. Hu, Z. Chen, Y. Jia, M. Wang, and T. Q. S. Quek, “Asymptotically optimal arrival rate for IoT networks with AoI and peak AoI constraints,” *IEEE Commun. Lett.*, vol. 25, no. 12, pp. 3853–3857, Dec. 2021.
- [14] C. Xu, H. H. Yang, X. Wang, and T. Q. S. Quek, “Optimizing information freshness in computing-enabled IoT networks,” *IEEE Internet Things J.*, vol. 7, no. 2, pp. 971–985, Feb. 2020.
- [15] J. P. Champati, R. R. Avula, T. J. Oechtering, and J. Gross, “Minimum achievable peak age of information under service preemptions and request delay,” *IEEE J. Sel. Areas Commun.*, vol. 39, no. 5, pp. 1365–1379, May 2021.
- [16] Z. Fang, J. Wang, C. Jiang, Q. Zhang, and Y. Ren, “AoI-inspired collaborative information collection for AUV-assisted Internet of Underwater Things,” *IEEE Internet Things J.*, vol. 8, no. 19, pp. 14559–14571, Oct. 2021.

- [17] C. Kam, S. Kompella, G. D. Nguyen, and A. Ephremides, "Effect of message transmission path diversity on status age," *IEEE Trans. Inf. Theory*, vol. 62, no. 3, pp. 1360–1374, Mar. 2016.
- [18] Y. Inoue, H. Masuyama, T. Takine, and T. Tanaka, "A general formula for the stationary distribution of the age of information and its application to single-server queues," *IEEE Trans. Inf. Theory*, vol. 65, no. 12, pp. 8305–8324, Dec. 2019.
- [19] A. Kosta, N. Pappas, A. Ephremides, and V. Angelakis, "The age of information in a discrete time queue: Stationary distribution and non-linear age mean analysis," *IEEE J. Sel. Area Comm.*, vol. 39, no. 5, pp. 1352–1364, May 2021.
- [20] X. Sun, F. Zhao, H. H. Yang, W. Zhan, X. Wang, and T. Q. S. Quek, "Optimizing age of information in random-access Poisson networks," *IEEE Internet Things J.*, vol. 9, no. 9, pp. 6816–6829, May 2022.
- [21] H. H. Yang, C. Xu, X. Wang, D. Feng, and T. Q. S. Quek, "Understanding age of information in large-scale wireless networks," *IEEE Trans. Wireless Commun.*, vol. 20, no. 5, pp. 3196–3210, May 2021.
- [22] N. Akar and O. Dogan, "Discrete-time queueing model of age of information with multiple information sources," *IEEE Internet Things J.*, vol. 8, no. 19, pp. 14531–14542, Oct. 2021.
- [23] R. D. Yates and S. K. Kaul, "The age of information: Real-time status updating by multiple sources," *IEEE Trans. Inf. Theory*, vol. 65, no. 3, pp. 1807–1827, Mar. 2019.
- [24] L. Huang and E. Modiano, "Optimizing age-of-information in a multi-class queueing system," in *Proc. IEEE Int. Symp. Inf. Theory*, Hong Kong, China, 2015, pp. 1681–1685.
- [25] Z. Chen et al., "Age of information: The multi-stream M/G/1/1 non-preemptive system," *IEEE Trans. Commun.*, vol. 70, no. 4, pp. 2328–2341, Apr. 2022.
- [26] E. Gindullina, L. Badia, and D. Gündüz, "Age-of-information with information source diversity in an energy harvesting system," *IEEE Trans. Green Commun. Netw.*, vol. 5, no. 3, pp. 1529–1540, Sep. 2021.
- [27] Y.-P. Hsu, E. Modiano, and L. Duan, "Scheduling algorithms for minimizing age of information in wireless broadcast networks with random arrivals," *IEEE Trans. Mobile Comput.*, vol. 19, no. 12, pp. 2903–2915, Dec. 2020.
- [28] C. Li, S. Li, Y. Chen, Y. T. Hou, and W. Lou, "Minimizing age of information under general models for IoT data collection," *IEEE Trans. Netw. Sci. Eng.*, vol. 7, no. 4, pp. 2256–2270, Dec. 2020.
- [29] L. Liu, X. Qin, X. Xu, H. Li, F. R. Yu, and P. Zhang, "Optimizing information freshness in MEC-assisted status update systems with heterogeneous energy harvesting devices," *IEEE Internet Things J.*, vol. 8, no. 23, pp. 17057–17070, Dec. 2021.
- [30] Y. Cai, S. Wu, J. Luo, J. Jiao, N. Zhang, and Q. Zhang, "Age-oriented access control in GEO/LEO heterogeneous network for marine IoT: A deep reinforcement learning approach," *IEEE Internet Things J.*, vol. 9, no. 24, pp. 24919–24932, Dec. 2022.
- [31] "LoRaWAN 1.1 specification," LoRa Alliance Tech. Committee, Fremont, CA, USA, Oct. 2017.
- [32] Y.-P. E. Wang et al., "A primer on 3GPP narrowband Internet of Things," *IEEE Commun. Mag.*, vol. 55, no. 3, pp. 117–123, Mar. 2017.
- [33] R. D. Yates and S. K. Kaul, "Status updates over unreliable multiaccess channels," in *Proc. IEEE Int. Symp. Inf. Theory*, 2017, pp. 331–335.
- [34] B. Yu, Y. Cai, and D. Wu, "Joint access control and resource allocation for short-packet-based mMTC in status update systems," *IEEE J. Sel. Areas Commun.*, vol. 39, no. 3, pp. 851–865, Mar. 2021.
- [35] D. C. Atabay, E. Uysal, and O. Kaya, "Improving age of information in random access channels," in *Proc. IEEE Conf. Comput. Commun. Workshops*, 2020, pp. 912–917.
- [36] O. T. Yavascan and E. Uysal, "Analysis of slotted Aloha with an age threshold," *IEEE J. Sel. Areas Commun.*, vol. 39, no. 5, pp. 1456–1470, May 2021.
- [37] X. Chen, K. Gatsis, H. Hassani, and S. S. Bidokhti, "Age of information in random access channels," *IEEE Trans. Inf. Theory*, vol. 68, no. 10, pp. 6548–6568, Oct. 2022.
- [38] W. Zhan, D. Wu, X. Sun, Z. Guo, P. Liu, and J. Liu, "Peak age of information optimization of slotted Aloha: FCFS versus LCFS," *IEEE Trans. Netw. Sci. Eng.*, vol. 10, no. 6, pp. 3719–3731, Nov./Dec. 2023.
- [39] Z. Jiang, S. Zhou, and Z. Niu, "Distributed policy learning based random access for diversified QoS requirements," in *Proc. IEEE Int. Conf. Commun.*, 2019, pp. 1–6.
- [40] G. Stamatakis, N. Pappas, and A. Tragantzis, "Optimal policies for status update generation in an IoT device with heterogeneous traffic," *IEEE Internet Things J.*, vol. 7, no. 6, pp. 5315–5328, Jun. 2020.
- [41] Z. Chen, N. Pappas, E. Björnson, and E. G. Larsson, "Optimizing information freshness in a multiple access channel with heterogeneous devices," *IEEE Open J. Commun. Soc.*, vol. 2, pp. 456–470, 2021.
- [42] N. Pappas and M. Kountouris, "Delay violation probability and age of information interplay in the two-user multiple access channel," in *Proc. IEEE Int. Workshop Signal Process. Adv. Wireless Commun. (SPAWC)*, 2019, pp. 1–5.
- [43] J. Wang, X. Jia, Z. Hao, and J. Yin, "Age of information optimization in heterogeneous multi-access cognitive radio networks," in *Proc. IEEE VTC2022-Spring*, Helsinki, Finland, 2022, pp. 1–5.
- [44] X. Wang and L. Duan, "Dynamic pricing and mean field analysis for controlling age of information," *IEEE/ACM Trans. Netw.*, vol. 30, no. 6, pp. 2588–2600, Dec. 2022.
- [45] A. Carleial and M. Hellman, "Bistable behavior of ALOHA-type systems," *IEEE Trans. Commun.*, vol. 23, no. 4, pp. 401–410, Apr. 1975.
- [46] L. Dai, "Stability and delay analysis of buffered Aloha networks," *IEEE Trans. Wireless Commun.*, vol. 11, no. 8, pp. 2707–2719, Aug. 2012.
- [47] T. Gao, Q. Tang, J. Li, Y. Zhang, Y. Li, and J. Zhang, "A particle swarm optimization with Lévy flight for service caching and task offloading in edge-cloud computing," *IEEE Access*, vol. 10, pp. 76636–76647, 2022.
- [48] D. Gross and C. M. Harris, *Fundamentals of Queueing Theory*. Hoboken, NJ, USA: Wiley, 1998.
- [49] W. Zhan and L. Dai, "Massive random access of machine-to-machine communications in LTE networks: Modeling and throughput optimization," *IEEE Trans. Wireless Commun.*, vol. 17, no. 4, pp. 2771–2785, Apr. 2018.
- [50] W. Zhan and L. Dai, "Access delay optimization of M2M communications in LTE networks," *IEEE Wireless Commun. Lett.*, vol. 8, no. 6, pp. 1675–1678, Dec. 2019.
- [51] A. Maatouk, S. Kriouile, M. Assaad, and A. Ephremides, "The age of incorrect information: A new performance metric for status updates," *IEEE/ACM Trans. Netw.*, vol. 28, no. 5, pp. 2215–2228, Oct. 2020.
- [52] R. D. Yates, Y. Sun, D. R. Brown, III, S. K. Kaul, E. Modiano, and S. Ulukus, "Age of information: An introduction and survey," *IEEE J. Sel. Area Comm.*, vol. 39, no. 5, pp. 1183–1210, May 2021.
- [53] Evolved Universal Terrestrial Radio Access (E-UTRA), Radio Resource Control (RRC) Protocol Specification; (Release 13), Version 13.12.0, 3GPP Sophia Antipolis, France, Rep. ETSI TS 36.331, Jan. 2019.
- [54] R. Eberhart and J. Kennedy, "A new optimizer using particle swarm theory," in *Proc. 6th Int. Symp. Micro Mach. Human Sci. (MHS)*, 1995, pp. 39–43.
- [55] J. Kennedy, "The particle swarm: Social adaptation of knowledge," in *Proc. Int. Conf. Evol. Comput.*, Indianapolis, IN, USA, 1997, pp. 303–308.
- [56] J. Kennedy, "Particle swarm optimization," in *Encyclopedia of Machine Learning*. New York, NY, USA: Springer, 2010, pp. 760–766.
- [57] M. Lovbjerg and T. Krink, "Extending particle swarm optimisers with self-organized criticality," in *Proc. Congr. Evol. Comput. (CEC)*, 2002, pp. 1588–1593.
- [58] J. Kennedy and R. Eberhart, "Particle swarm optimization," in *Proc. IEEE Int. Conf. Neural Netw.*, 1995, pp. 1942–1948.



DEWEI WU received the B.E. degree in communication engineering from the School of Electronics and Communication Engineering, Sun Yat-sen University, Shenzhen, China, in 2021, where he is currently pursuing the M.E. degree in information and communication engineering with the School of Electronics and Communication Engineering. His research interests include age of information, Internet of Things, and stochastic modeling of wireless network.



WEN ZHAN (Member, IEEE) received the B.S. and M.S. degrees from the University of Electronic Science and Technology of China, China, in 2012 and 2015, respectively, and the Ph.D. degree from the City University of Hong Kong, China, in 2019, where he was a Research Assistant and a Postdoctoral Fellow. Since 2020, he has been with the School of Electronics and Communication Engineering, Sun Yat-sen University, China, where he is currently an Associate Professor. His research interests include the Internet of Things, modeling, and performance optimization of next-generation mobile communication systems.



XINGHUA SUN (Member, IEEE) received the B.S. degree from the Nanjing University of Posts and Telecommunications (NJUPT), China, in 2008, and the Ph.D. degree from the City University of Hong Kong (CityU), China, in 2013. In 2010, he was a visiting student with the National Institute for Research in Digital Science and Technology, France. In 2013, he was a Postdoctoral Fellow with CityU. From 2015 to 2016, he was a Postdoctoral Fellow with the University of British Columbia, Canada. From July to August 2019, he was a Visiting Scholar with the Singapore University of Technology and Design, Singapore. From 2014 to 2018, he was an Associate Professor with NJUPT. Since 2018, he has been an Associate Professor with Sun Yat-sen University, Shenzhen, Guangdong, China. His research interests include stochastic modeling and optimization of wireless networks and machine learning for networking. He was a co-recipient of the Best Paper Award from the EAI IoTaaS in 2023. He served as a technical program committee member and an organizing committee member for numerous conferences.



JINGJING LIU (Member, IEEE) received the B.Eng. (first Class Hons.) and M.Eng. degrees from the School of Electrical and Electronic Engineering, Nanyang Technological University, Singapore, in 2003 and 2005, respectively, and the D.Phil. degree from the Department of Engineering Science, University of Oxford, Oxford, U.K., in 2009, where he was a Postdoctoral Research from 2009 to 2010. He was a Researcher with Peking University Shenzhen Research Institution for a few years. He is currently an Associate Professor with Sun Yat-sen University, Shenzhen, China. His research interests include low-power smart micro-sensor integrated circuit design, image sensors, biomedical sensors, and energy harvesting circuits.



ZHIHENG LI received the B.S. degree from the University of Science and Technology of China, China, in 2022, where he was a Research Assistant. His research interests include data analysis and processing, and machine learning.